CONFERENCE PRE-PRINT

PROGRESS OF LOWER HYBRID CURRENT DRIVE EXPERIMENT TOWARDS LONG-PULSE OPERATION ON EAST

M.H. Li, W.W. Zhang, J.L. Chen, C.B. Wu, B.J. Ding, M. Wang, L. Liu, L.M. Zhao, W.D. Ma, Y. Yang, Z.G. Wu, L. Yin, J. Huang, J.P. Qian, X.Z. Gong Institute of Plasma Physics, Chinese Academy of Sciences

Hefei, China

Email: mhli@ipp.ac.cn

Y. Savoye-Peysson, J. Hillairet, and A. Ekedahl CEA, IRFM Saint-Paul-lez-Durance, France

Abstract

Recent achievements of lower hybrid current drive (LHCD) system at 4.6 GHz in high-power and long-pulse operation on EAST tokamak are reported. The duration of long-pulse plasmas has been extended to 1056 s with 1.1 MW LH power in I-mode and 1066 s with 0.92 MW in H-mode. The domains in plasma current (I_p) and line-averaged plasma density (\bar{n}_e) of fully non-inductive discharges with LHCD alone and with the combined LHCD and electron cyclotron resonant heating (ECRH) are presented. The LHCD efficiency (η_{CD}) with different plasma densities in both L- and H-mode discharges characterized by residual loop voltage $V_{loop} = 0$ is obtained. The experimental results show that the CD efficiency is improved significantly by ECRH due to the increase of electron temperature. Limitations for high power coupling and high CD efficiency of LH waves are summarized and discussed, including the hot spots or arc issues in front of the antenna, and the deteriorated heating and current drive (H&CD) effects with high heating power when the plasma confinement becomes poor. Finally, prospects with a new 4 MW LHCD system at 4.6 GHz which is under development and future work to further understand the experimental observations are given.

1. INTRODUCTION

LHCD has a very high CD efficiency with respective to other non-inductive methods [1]. EAST is a mediumsized tokamak with the major radius $R \sim 1.9$ m, minor radius $a \sim 0.45$ m, magnetic field $B_t \sim 2.5$ T, which aims at long-pulse operation in support of ITER and CFETR. LHCD system operating at 4.6 GHz plays a very important role in steady-state long-pulse operation on EAST. It adopts a full active multijunction (FAM) launcher arranged in an array of four rows and six columns, as shown in Fig. 1 [2]. Each row consists of six modules and each



FIG. 1. LHCD FAM launcher at 4.6 GHz with tungsten guard limiters.

module is powered by one 250 kW CW klystron separately. The total twenty-four modules result in 6 MW nominal power of the system. Guard limiters made of graphite tiles were upgraded to tungsten blocks with improved cooling in 2017 [3]. The nominal parallel refractive index (N_{\parallel}) peaks at 2.04 and the first main N_{\parallel} of the power

spectrum can be varied from 1.7 to 2.5 by adjusting the phasing between adjacent modules [4]. The power directivity (D_p) defined as the power at $N_{\parallel} < 0$ (driving counter current) divided by the total power is as high as 76%.

2. ADVANCES IN STEADY-STATE LONG-PULSE EXPERIMENT

The operational domains in the pulse duration versus the LH power (P_{LH}) coupled into plasmas from 2014 (the first plasma operation) are illustrated in Fig. 2. It is seen that the LH power injected into plasmas decreases significantly as the pulse duration increases. Typical long-pulse achievements are: 1056 s with 1.1 MW in I-mode [5], 1066 s with 0.92 MW in H-mode [6]. Before 2017, the guard limiters consisted of graphite tiles plated with silicon carbide. Due to the poor contact between the heat sink and the graphite tiles, the thermal transfer efficiency was low. As a result, the designed target of the heat flux was only $\sim 2.0 \text{ MW/m}^2$ [7]. When operating with LH power larger than 2.0 MW, strong hot spots and are events were often observed on the guard limiters which will be shown in the latter content. In order to increase the power handling capability, the guard limiters were upgraded to tungsten with actively cooling structures in 2017 [3]. Explosive welding technology was applied for fabricating the connecting water tanks. The tungsten block was designed to be a wedge-shape in the toroidal cross section in order to reduce the averaged heat flux. Calculations indicate this tungsten guard limiter can operate at peak power density of 12.9 MW/m². With these new tungsten protection limiters, the coupled power was substantially enhanced. Coupled power in the range of 2.5 - 2.8 MW with pulse length ~ 10 s can be achieved routinely. The maximum LH power coupled into L-mode plasmas reached 3.7 MW (see Fig. 3), corresponding to the power

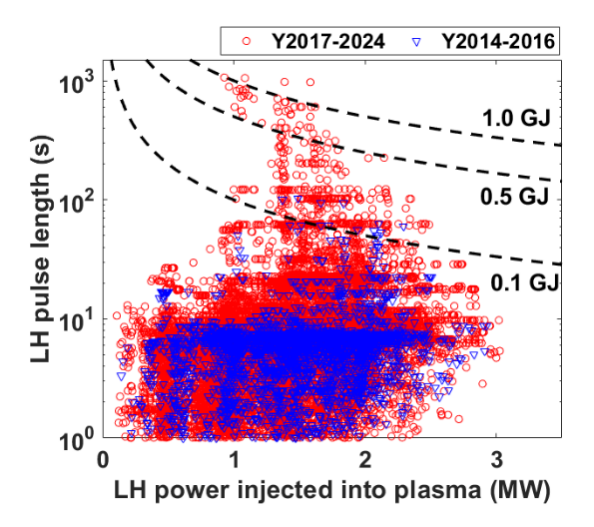


FIG. 2. LH pulse length versus power level injected into plasma from the first operation in 2014.

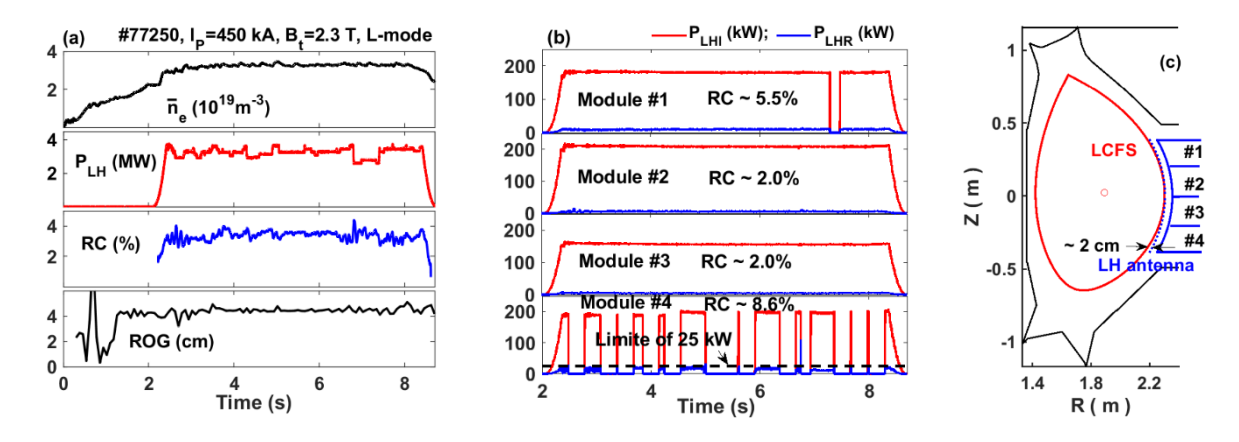


FIG. 3. Typical waveform of high-power operation with 4.6 GHz LH waves in EAST L-mode discharge (a); Coupling property of one klystron module at each row (b). Magnetic equilibrium configuration of discharge #77250 (c). \bar{n}_e lineaveraged density, P_{LH} LH power coupled into plasmas, RC power reflection coefficient defined as P_{LHR} / P_{LHI} , ROG radial out gap between LCFS and LH antenna, P_{LHI} incident power, P_{LHR} reflected power by the plasmas, LCFS lost closed flux surface.

density ~ 22.6 MWm⁻² and $\sim 65\%$ of the total nominal power. Note that only 23 klystrons (namely, the total source power is 23×250 kW = 5.75 MW) are available for this experiment. This ratio is similar to other LHCD systems [8], such as on JET at 3.7 GHz, JT-60U at 1.74 - 2.23 GHz and Tore Supra at 3.7 GHz, as depicted in Fig. 4. However, many power trips exists in this discharge due to the mismatch between the magnetic flux surface and the antenna shape. As a result, the averaged LH power (over the pulse length) was only 3.0 MW in Fig. 2. Although the reflection coefficients (RC) of the two middle modules remain as low as 2%, the coupling of the top and in particular the bottom modules are much worse. The RC of the bottom module is as high as $\sim 8.6\%$ and the reflected power (P_{LHR}) reaches the limit of 25 kW, triggering the protection system.

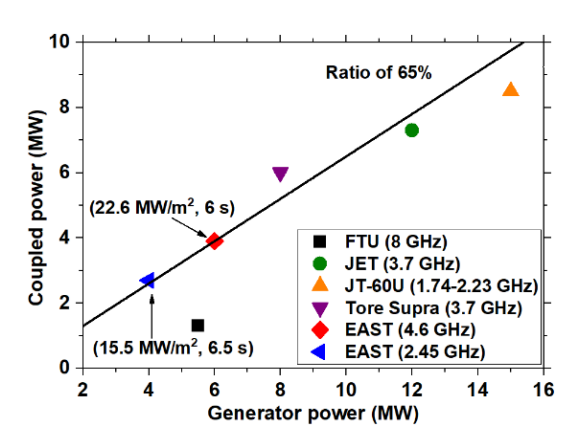


FIG. 4. Maximum LH power coupled into plasmas versus generator power on EAST and other tokamaks. The data of other tokamaks are quoted from reference [8].

Fig. 5 represents the domains in plasma current (I_p) and line-averaged density (\bar{n}_e) of steady-state discharges (loop voltage $V_{loop} = 0$) with LHCD alone and with the combination of LHCD + ECRH/ECCD. It is seen that the fully non-inductive L-mode discharges are limited by $\bar{n}_e \le 2.8 \times 10^{19} \text{m}^{-3}$ and $I_p \le 470$ kA with LH only, while the density is extended to $3.1 \times 10^{19} \text{m}^{-3}$ with both the LH and EC waves heating. In H-mode, steady-state plasmas have been achieved with the density up to $4.5 \times 10^{19} \text{m}^{-3}$ and moderate plasma current ($I_p = 370 \text{ kA}$).

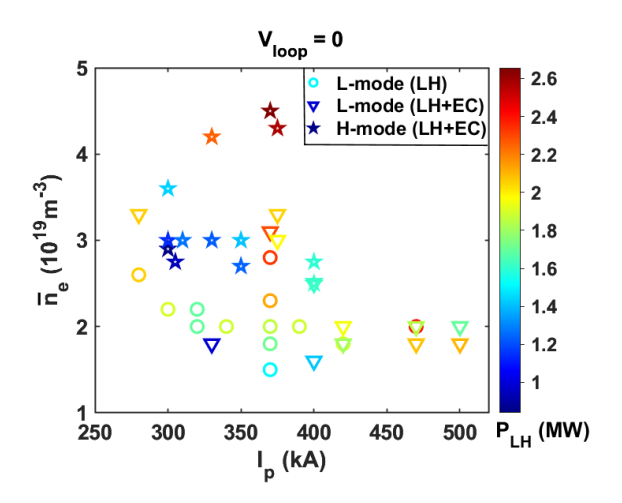


FIG. 5. Domains in plasma current (I_p) and line-averaged density (\bar{n}_e) of steady-state discharges with LHCD and ECRH/ECCD. Colour bar indicates the LH power.

LHCD efficiency defined as

$$\eta_{\rm CD} = \frac{I_{\rm LH} \bar{n}_{\rm e} R}{D_{\rm p} P_{\rm LH}} ({\rm Am^{-2} W^{-1}})$$
(1)

in steady-state L- and H-mode plasmas with different plasma densities is shown in Fig 6, where I_{LH} the driven current by LH wave, and D_p the power directivity of the antenna. Assuming $I_{LH} = I_p$, the CD efficiency is much higher in H-mode than in L-mode (see Fig. 6a), indicating considerable bootstrap current in H-mode. The precise LHCD efficiency is shown in Fig. 6b with the LH driven current calculated by $I_{LH} = I_p - I_{EC} - I_{BS}$, where I_{EC} and I_{BS} are EC driven current and bootstrap current, respectively. These two current components are predicted by TORAY code and Sauter model with the experimental kinetic profiles. It is seen that the CD efficiency is improved

significantly by ECRH in L-mode due to the increase in electron temperature (T_e). In H-mode, the CD efficiency is as high as $\sim 1.15 \times 10^{19}$ (A/W/m²) with the line-averaged density around 2.9×10^{19} m⁻³, while it drops slightly with density increasing. The comparison between the experimental CD efficiency and the prediction with ray-tracing / Fokker-Planck suit codes is under way.

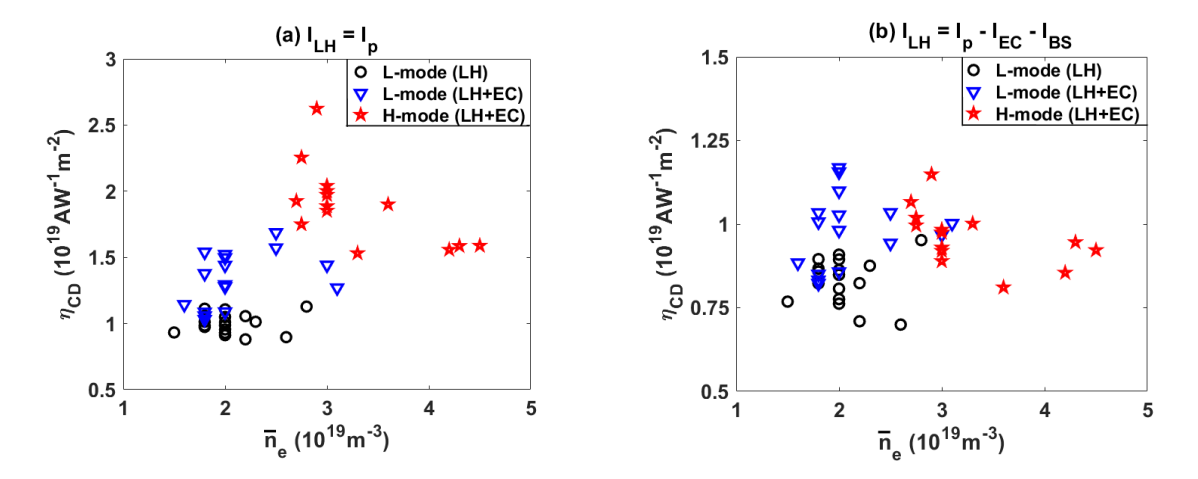


FIG. 6. LHCD efficiency (η_{CD}) as a function of line-averaged density (\bar{n}_e) with the assumption of LH current $I_{LH} = I_p$ (a), and LH current calculated by $I_{LH} = I_p - I_{EC} - I_{BS}$ (b).

3. LIMITATIONS TOWARDS HIGH-POWER AND LONG-PULSE OPERATION

For a multijunction antenna, the very high parallel index $N_{\parallel} (\geq 20)$ components are intrinsic in the radiated power spectrum, which can be absorbed by electrons with several tens of keV in front of the antenna through Landau damping [9]. Because the radial width of these fast electrons accelerated by the high N_{\parallel} components is much narrow (usually less than 5 mm), the heat flux in front of the launcher but very close to the antenna mouth can be as high as ~ dozens of MWm⁻² [10]. As a result, strong hot spots are generated on the guard limiters of the antenna and also on other plasma facing components magnetically connected to the antenna. Previous study reveals that the radial width of the strong heat flux on EAST is only 2 mm [11] which is consistent with the prediction by a simple wave propagation model [12]. Local hot spot issue on both guard limiters is a serious problem for highpower operation since the heat flux increases almost linearly with P_{LH} [13]. Meanwhile, when the RF field exceeds a critical value, the electrons can gain enough energy during their passes between the waveguide walls to yield secondary electrons from the surface, leading to electron avalanche. The breakdown is more likely to occur at the plasma - waveguides interface due to the fact that the higher order (evanescent) TM modes excited in this location will maximize the E-field at the grill mouth [14]. If the breakdown transits to an arc event, it can cause severe damage to the waveguides surface and also produce large impurity release, which may eventually lead to a plasma disruption. Strong hot spots usually lead to arc events due to the fact that thermo-ionic effect could lower the threshold for breakdown at high temperature. Figs. 7 and 8 show an example of L-mode discharge disrupted by

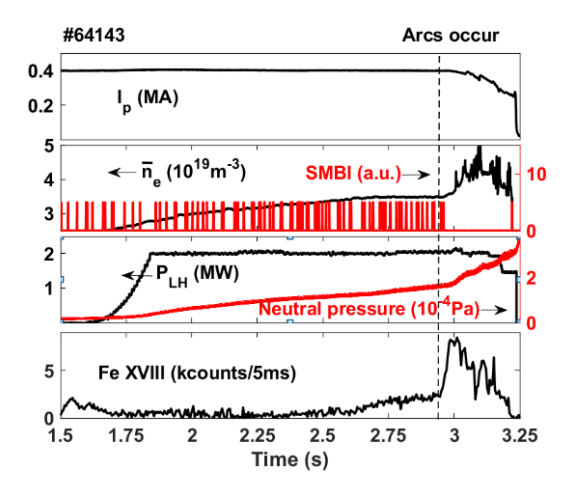


FIG. 7. Time evolution of several key plasma parameters during a L-mode discharge disrupted by hot spot and arc events. SMBI supersonic molecular beam injection and Fe XXIII iron 22+.

hot spot and arc events which was performed with the graphite guard limiters before 2017. About 0.4 s after the LH power injection, a small hot spot appears on the right limiter (viewing from the plasmas). Subsequently, the area of hot spot gets larger and the brightness become stronger, suggesting that the surface temperature increases with time. An arc event occurs at t = 2.94 s, followed by a sharp increase of iron radiation, which is one kind of material of LH antenna. In addition, the neutral pressure increases significantly during the arc as a consequence of the significant out gassing of the antenna. Finally, the plasma is disrupted at t = 3.2 s due to large iron impurity flux. Strong erosions on the right limiter and surface melting on the waveguides are observed after the plasma experiment. Experimental results on Tore Supra [10] and EAST [15] have shown the strong dependence of heat flux on electron density at the antenna mouth. This implies that in principle the electron density should be controlled carefully at the lower limit for optimal coupling. In this paper, it is found that the hot spots show weak

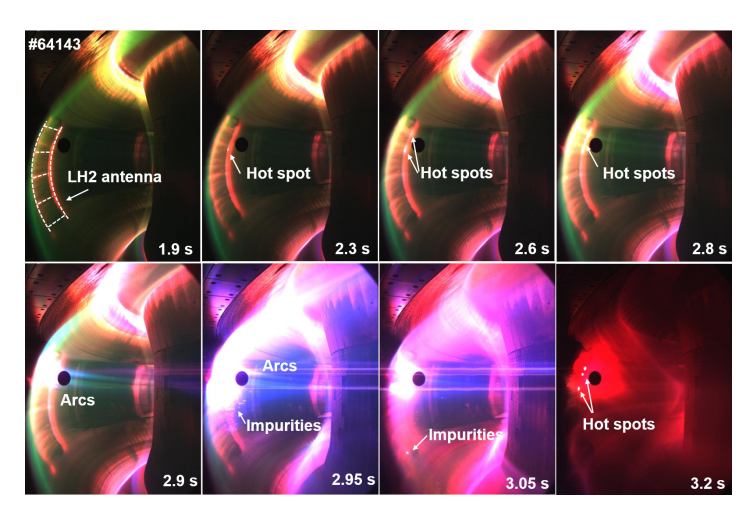
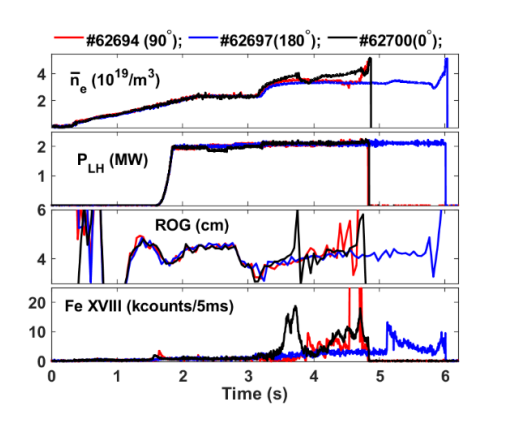


FIG. 8. Photos taken by CCD camera at different time points showing the hot spot and arc events.

dependence on the antenna phasing and effective antenna width, as evidenced in Fig. 9. This may be ascribed to the weak dependence of high N_{\parallel} fraction on the antenna phasing, as shown in Fig. 10, which is calculated by a



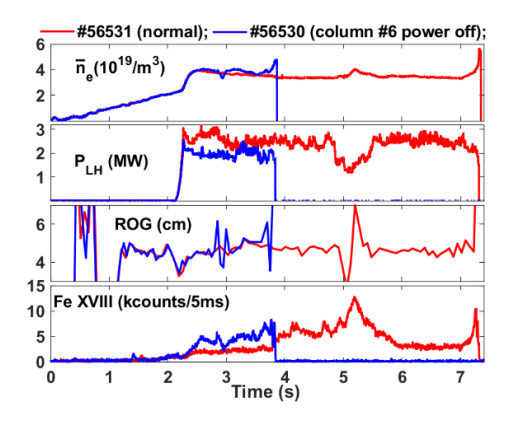


FIG. 9. Effects of antenna phasing (a) and effective antenna width (b) on the hot spot and arc events.

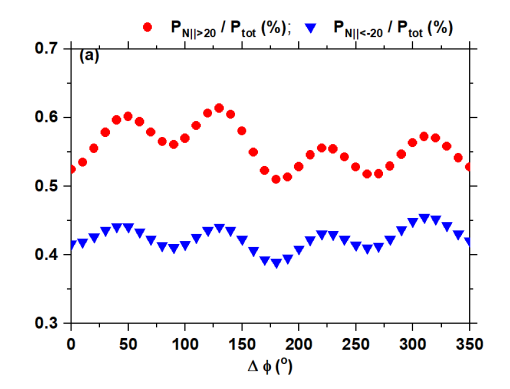


FIG. 10. Ratio of high N_{\parallel} components to total power.

linear coupling code ALOHA [16]. Although the total power is lower for the discharge #56530 with column #6 power off, the plasma is terminated by the hot spot issue as well, indicating that the power density (i.e. the electric field) plays an important role rather than the total power level. According to the calculation in [10], the speed of fast electrons will saturate after accelerating through 20 waveguides. From this, it has been inferred that the hot spot on EAST would be mitigated with only two columns power on (each column contains 8 waveguides in toroidal direction).

Another limitation for achieving steady-state operation is the anomalous loss of LHCD efficiency at high heating power. Fig. 11 shows the statistical data of plasma stored energy ($W_{\rm MHD}$) normalized by $I_p^{0.85}\bar{n}_e^{0.1}B_t^{0.2}$ according to the ITER89-P scaling law [17] as a function of the total heating power in L-mode plasmas. It is clear that the plasma heating effect is saturated when $P_{\rm LH} > 2$ MW. As is well known, the lifetime of fast electrons depends on

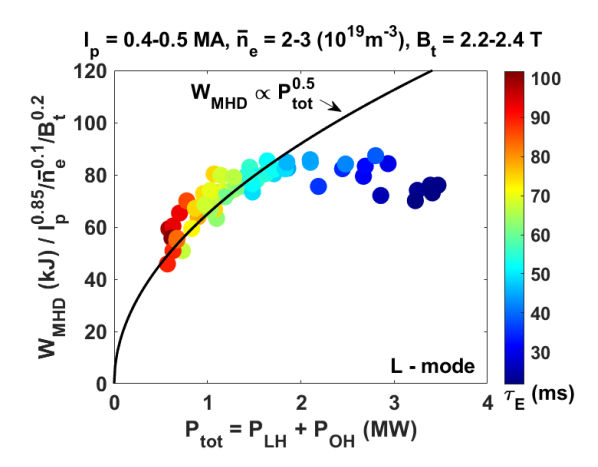


FIG. 11. Plasma stored energy (W_{MHD}) normalized by $I_p^{0.85} \bar{n}_e^{0.1} B_t^{0.2}$ as a function of the total heating power (ohmic and LH) in L-mode plasmas.

the balance between the collisional slowing down and the radial diffusion time-scale [18]. With the heating power increasing, the plasma confinement is degraded, leading to a stronger radial transport of fast electrons. The direct fast electron loss due to radial transport may play an important role in the CD efficiency on small or medium-sized devices, as observed in [19]. Moreover, no H&CD effects of LH waves were observed when the LH power was added to target H-mode plasmas sustained by $P_{\text{NBI}} + P_{\text{EC}} = 3.85$ MW with high plasma density ($\bar{n}_e = 4.3 \times 10^{19} \text{m}^{-3}$) (see Fig. 12). Although these discharges are in H-mode, the confinement time is not high ($\tau_{\text{E}} \le 45$ ms). This adverse phenomenon is not well understood at present. Direct fast electron loss and power dissipation in SOL by non-resonant collision may be the candidates. Modelling results show that significant power loss exists in Alcator C-Mod [20] and FTU [21] high-density experiments, which could be responsible for the CD degradation.

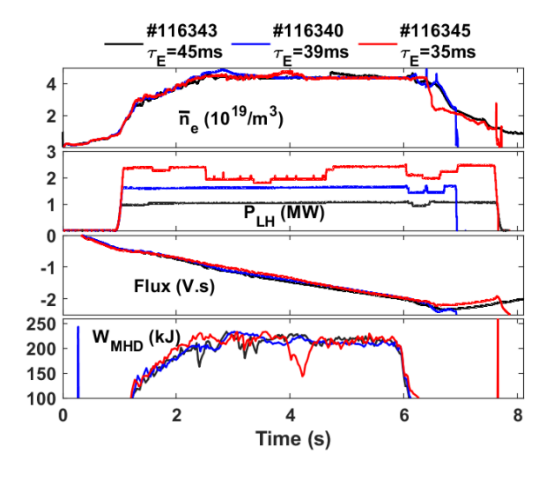


FIG. 12. Comparison of LH heating and current drive effects with different power levels in H-mode. Other parameters are $I_p = 0.5$ MA, $B_t = 2.4$ T, $P_{EC} = 0.85$ MW, $P_{NBI} = 3.0$ MW.

4. CONCLUSION AND PROSPECT

LHCD system operating at 4.6 GHz is the main non-inductive tool for long-pulse operation on EAST. Thanks to the upgraded tungsten guard limiters which has much better cooling effect than the old graphite, significant progress has been achieved recently in high-power long-pulse operation. Better cooling means reduced hot spots and associated sputtering, then less arcs, which in return allows increasing the coupled power. The pulse length of LH system at 4.6 GHz has been extended to 1056 s with 1.1 MW in I-mode and 1066 s with 0.92 MW in H-mode. Fully non-inductive plasmas with the LHCD alone and the combined LHCD + ECRH/ECCD have been obtained in a wide range of plasma current $I_p = 280$ - 500 (kA) and line-averaged electron density $\bar{n}_e = 1.5$ - 4.5 (10¹⁹m⁻³). Benefiting from the electron temperature effects by ECRH [22] and other methods such as lithium coating [23], favourable B_t direction (the ion ∇B drift towards the primary X-point) [24], LHCD efficiency normalized by the power directivity (D_p) in the H-mode reaches ~ 1.15 (10¹⁹ A/W/m²) with $\bar{n}_e \sim 2.9 \times 10^{19} \text{m}^{-3}$, and it drops slightly with electron density increasing.

Hot spots / arc issues in front of the LH launcher are the main factors limiting the power handling performance in long-pulse plasmas. The past experiments have demonstrated a strong sensitivity of the heat flux to the LH power and electron density at the antenna mouth. In this paper, it is found that the hot spot events are weakly dependent on the antenna phasing and the effective antenna width. Anomalous loss of LH heating and current drive effects under the condition of high heating power is another limitation to extent the steady-state scenarios. The underlying mechanisms accounting for this CD efficiency degradation will be studied in the future.

A new LH system with active cooling passive active multijunction (PAM) launcher (see Fig. 13) at 4.6 GHz is under development [25]. The PAM with an optimized radius of poloidal curvature will be fed by eight 500 kW/CW klystrons each with two output windows, generating a total nominal power of 4 MW. Simulated results [26] with ALOHA code indicate that the optimum coupling could be expected around the cut-off density, which is very attractive for long-pulse operation. The new system is scheduled for the plasma experiment in the first half of 2026. Long-pulse scenarios with higher plasma parameters can be foreseen.

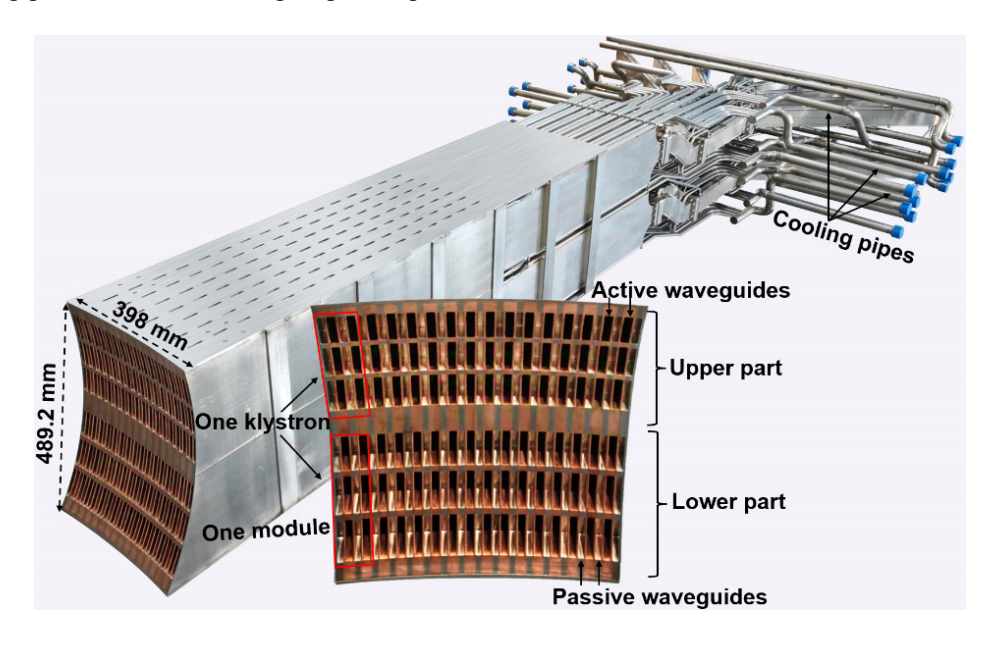


FIG. 13. A new PAM antenna at 4.6 GHz waiting for installation on EAST tokamak.

ACKNOWLEDGEMENTS

This work was supported by the National Natural Science Foundation of China (Grant Nos. 12475231, 11975266, and 12405270), upgrade and renovation of superconducting Tokomak Nuclear Fusion experimental device No. 2406-000000-04-02-630302, and the Comprehensive Research Facility for Fusion Technology Program of China under Contract No. 2018-000052-73-01-001228.

REFERENCES

- [1] USHIGUSA, K., et al., Lower hybrid current drive efficiency in the JT-60 tokamak, Nucl. Fusion 29 (1989) 1052.
- [2] LIU L., et al., 4.6-GHz LHCD Launcher System of Experimental Advanced Superconducting Tokamak, Fusion Sci. Technol. **75** (2019) 49.
- [3] ZHANG L.L., et al., A tungsten guard limiter for EAST 4.6 GHz lower hybrid waveguide antennas, Fusion Eng. Des. 136 (2018) 447.
- [4] LI M.H., et al., Comparative modeling of lower hybrid wave coupling with 2.45 GHz and 4.6 GHz launchers on EAST, AIP Conference Proceedings **2254** (2020) 080005.
- [5] SONG Y.T., et al., Realization of thousand-second improved confinement plasma with Super I-mode in Tokamak EAST, Sci. Adv. 9 (2023) eabq5273.
- [6] GONG X.Z., et al., Overview of recent experimental results on EAST in support of ITER new research plan, 30th IAEA Fusion Energy Conference, Chengdu, China, Oct 13 18, 2025.
- [7] LIU C.L., et al., Current status and upgrade activities on the guard limiter of 4.6 GHz lower hybrid antennas for EAST tokamak, Fusion Eng. Des. **125** (2017) 93.
- [8] ITER Physics Expert Group on Energetic Particles, Heating and Current Drive, Chapter 6: Plasma auxiliary heating and current drive, Nucl. Fusion **39** (1999) 2495.
- [9] BRAMBILLA M., Electron Landau damping of lower hybrid waves, Nucl. Fusion 18 (1978) 493.
- [10] GONICHE M., et al., Enhanced heat flux in the scrape-off layer due to electrons accelerated in the near field of lower hybrid grills, Nucl. Fusion **38** (1998) 919.
- [11] WANG M., et al., Improvement of lower hybrid current drive systems for high-power and long-pulse operation on EAST, Nucl. Eng. Technol. **54** (2022) 4102.
- [12] RANTAMAKI K.M., et al., Estimation of heat loads on the wall structures in parasitic absorption of lower hybrid power, Nucl. Fusion **40** (2000) 1477.
- [13] JACQUET P., et al., Heat loads on JET plasma facing components from ICRF and LH wave absorption in the SOL, Nucl. Fusion **51** (2011) 103018.
- [14] FUCHS V., et al., Interaction of tokamak edge electrons with lower hybrid antenna electric field spectra, Plasma Phys. Control. Fusion **41** (1999) A495.
- [15] DING B.J., et al., Effect of edge plasma density on hot spot in LHCD plasma in EAST, Nucl. Mater. Energy 27 (2021) 100992.
- [16] HILLAIRET J., et al., ALOHA: an Advanced LOwer Hybrid Antenna coupling code, Nucl. Fusion 50 (2010) 125010.
- [17] YUSHMANOV P.N., et al., Scalings for tokamak energy confinement, Nucl. Fusion 30 (1990) 1999.
- [18] PEYSSON Y., Transport of fast electrons during LHCD in TS, JET, and ASDEX, Plasma Phys. Control. Fusion **35** (1993) B253.
- [19] TAKASE Y., et al., Energy confinement studies of lower hybrid current driven plasmas in the Alcator C tokamak, Nucl. Fusion 27 (1987) 53.
- [20] WALLACE G.M., et al., Absorption of lower hybrid waves in the scrape off layer of a diverted tokamak, Phys. Plasmas 17 (2010) 082508.
- [21] BARBATO E., The role of non-resonant collision dissipation in lower hybrid current driven plasmas, Nucl. Fusion **51** (2011) 103032.
- [22] LI M.H., et al., Plasma heating by electron cyclotron wave and the temperature effects on lower hybrid current drive on EAST, Nucl. Fusion **63** (2023) 046019.
- [23] GONICHE M., et al., Influence of Li conditioning on Lower Hybrid Current Drive efficiency in H-mode and L- mode plasmas on EAST, EPJ Web of Conferences **157** (2017) 03018.
- [24] LI M.H., et al., Lower hybrid current drive efficiency in H-mode plasmas on EAST tokamak, AIP Conference Proceedings **2984** (2023) 090005.
- [25] LIU L., et al., Advances in lower hybrid technology at 4.6 GHz towards its application on CFETR, Plasma Sci. Technol., (under review).
- [26] LI M.H., et al., Design and analysis of a PAM launcher at 4.6 GHz for a new LHCD system on EAST, Nucl. Fusion 64 (2024) 036017.